



# Imaging acoustic vibrations in an ear model using spectrally encoded interferometry



Sveta Grechin, Dvir Yelin \*

Faculty of Biomedical Engineering, Technion—Israel Institute of Technology, Haifa 32000, Israel

## ARTICLE INFO

### Keywords:

Doppler imaging  
Interferometric imaging  
Optical design of instruments  
Biomedical imaging

## ABSTRACT

Imaging vibrational patterns of the tympanic membrane would allow an accurate measurement of its mechanical properties and provide early diagnosis of various hearing disorders. Various optical technologies have been suggested to address this challenge and demonstrated *in vitro* using point scanning and full-field interferometry. Spectrally encoded imaging has been previously demonstrated capable of imaging tissue acoustic vibrations with high spatial resolution, including two-dimensional phase and amplitude mapping. In this work, we demonstrate a compact optical apparatus for imaging acoustic vibrations that could be incorporated into a commercially available digital otoscope. By transmitting harmonic sound waves through the otoscope insufflation port and analyzing the spectral interferograms using custom-built software, we demonstrate high-resolution vibration imaging of a circular rubber membrane within an ear model.

© 2017 Elsevier B.V. All rights reserved.

## 1. Introduction

By transferring air pressure waves to bone vibrations, the tympanic membrane plays a key role in the human hearing process, with unique anatomy that allows it to receive acoustic waves with amplitudes as small as 20  $\mu\text{Pa}$  [1]. Partial loss of sensitivity to acoustic stimulation could be the result of tympanic membrane perforations [2], ear infection, fluid accumulation in the middle ear [3], hemangioma of the tympanic membrane [4] and congenital cholesteatoma [5]. In addition, being highly sensitive to its mechanical properties and surroundings, the tympanic membrane dynamics is strongly dependent on physiological changes in its environment. Sensing the full vibrational patterns of the tympanic membrane could thus serve as a direct diagnostic tool for outer and middle ear pathologies, and could also assist surgical intervention procedures including myringoplasty and tympanoplasty that depend on detailed inspection of the tympanic membrane.

Optical interferometry is currently the most sensitive approach for safely and accurately measuring tissue acoustic vibrations. Laser Doppler vibrometry allows high-sensitivity measurements of sub-nanometer axial displacements of a single point on the tympanic membrane [6,7]. Three-dimensional imaging of the acoustic vibrations in an excised (*ex vivo*) tympanic membrane was demonstrated using optical coherence tomography, by scanning the membrane

point-by-point [8]. Resolving the relative oscillation phases at all points on a membrane *in vivo*, however, could be challenging with this approach due to the lengthy scanning time and the size and weight of the scanning mechanism. Full-frame *ex vivo* measurement of the motion of a surgically exposed and white-painted tympanic membrane within a fresh temporal bone was demonstrated at discrete phase delays between laser pulses using stroboscopic holography [9]; *in vivo* imaging is yet to be demonstrated with this technique, but could be challenging due to the relative complexity of the holographic imaging apparatus.

Using single-shot imaging of a transverse line with slow single-axis scanning, interferometric spectrally encoded endoscopy [10] captures high-resolution images through a single-fiber imaging probe. Using high-speed line cameras, nanometer-scale axial displacements were imaged across two-dimensional vibrating surfaces [11]. A bench-top system that employs sophisticated processing of the acquired spectral interferograms has recently been demonstrated [12], allowing the recovery of a two-dimensional vibrational motion. In this work, we employ a novel design of our spectrally encoded acoustic imaging system as part of a commercially available digital otoscope, and demonstrate vibrational imaging inside an ear model with approximately 4.5-mm-diameter field of view and up to 0.6 nm axial resolution.

\* Corresponding author.

E-mail address: [yelin@bm.technion.ac.il](mailto:yelin@bm.technion.ac.il) (D. Yelin).

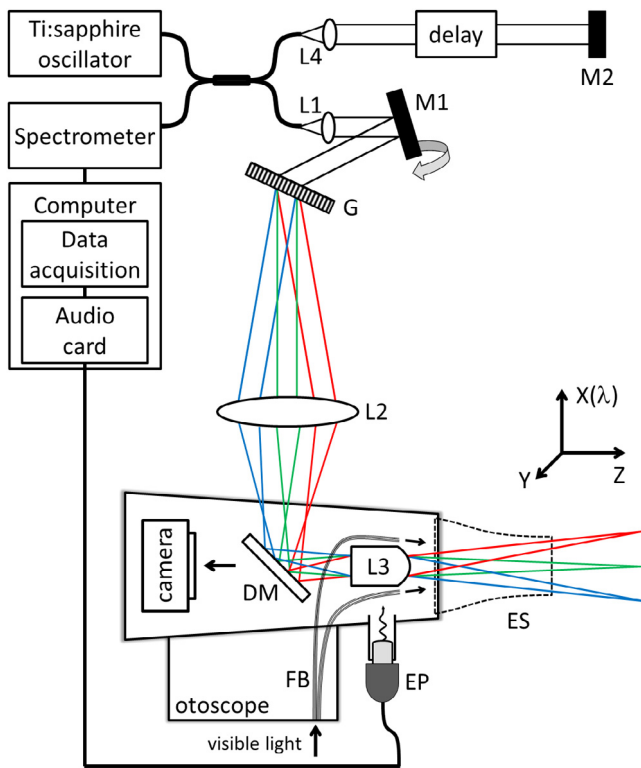


Fig. 1. Spectrally encoded vibration imaging system integrated into a digital otoscope. L1, L2, L4—lenses, L3—otoscope integral lens system, M1, M2—mirrors, G—diffraction grating, DM—dichroic mirror, EP—ear phone, FB—fiber bundle, ES—ear specula.

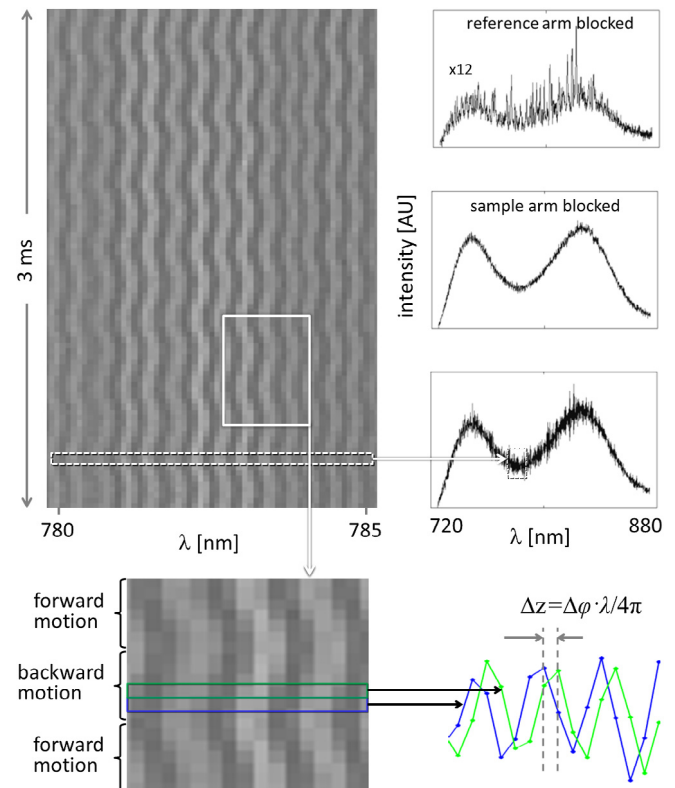


Fig. 3. Interferometric raw data obtained at 20 kHz from a single line on a membrane vibrating at 2.1 kHz. (For interpretation of the references to colour in this figure legend, the reader is referred to the web version of this article.)

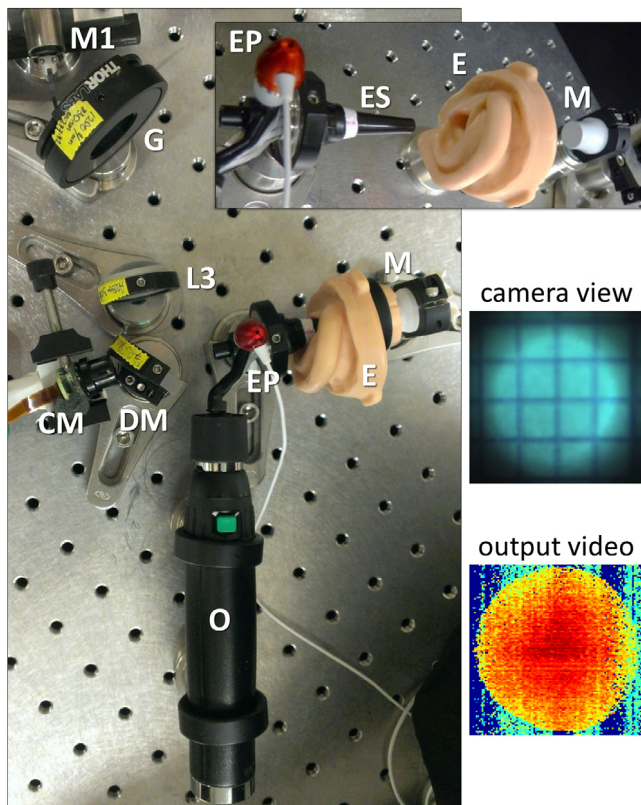


Fig. 2. Photograph of the optical system: O—otoscope handle, M1—scanning mirror, G—grating, L3—achromatic lens, DM—dichroic mirror, CM—otoscope camera, EP—ear phones, E—anatomic ear model, M—membrane, ES—ear specula.

## 2. Experimental setup

The experimental setup for imaging acoustic vibrations (Fig. 1) was modified from our previous work [12] to allow integration into the optical path of a commercially available digital otoscope (Digital macroview, Welch Allyn). Broadband (130 nm) light from a titanium sapphire oscillator (Femtolasers Rainbow, 800 nm center wavelength) was coupled into a 50/50 single-mode fiber coupler, collimated by an achromatic 11-mm-focal length lens (L1), deflected by a single-axis galvanometric scanning mirror (Cambridge Technology, M1), diffracted by a 1200 lines/mm transmission grating (Wasatch photonics, G), and imaged onto the back aperture of the otoscope 5-mm-diameter original lens system (L3) using a 30-mm-focal length achromatic lens (L2). A long-pass dichroic mirror (750 nm cutoff wavelength) was placed inside the otoscope optical path after removing its plastic casing for coupling the near-infrared beam into the otoscope optical path. The light was focused by the otoscope lens system to a 4.5-mm-wide transverse spectrally encoded line with a working distance of approximately 25 mm from the front aperture of the otoscope lens. Light reflected from the sample propagated back through the same optical path and coupled back into the fiber coupler. The resulting spectral line ( $x$  axis) was slowly scanned by the mirror M1 in the perpendicular  $y$  axis, covering a lateral field of view of approximately  $4.5 \text{ mm} \times 4.5 \text{ mm}$  with  $630 \times 630$  resolvable points [13] and a lateral resolution of approximately  $7 \mu\text{m}$  (FWHM). The reference arm of the Michelson interferometer comprised of a collimating 11-mm-focal length lens (L4) and a mirror (M2) mounted on a linear translation stage. Spectral interferograms were recorded using a custom-built spectrometer, comprised of a collimating 50-mm-focal length lens, a 1800 lines/mm transmission diffraction grating, a multielement focusing lens (Nikon, 85 mm focal length) and a high-speed line CMOS camera (Sprint sPL4096-70k, Basler Vision, 4096 pixels, 70 kHz maximum line rate). Two polarization controllers (not

shown in Fig. 1) were used at the two fiber coupler arms to increase interference contrast. The spectral resolution of the spectrometer was approximately 0.07 nm, over 3-times higher than that of the sample arm (0.21 nm). Single-frequency harmonic sound waves were synthesized by the computer audio card (built-in Intel high-definition audio) and generated by a single earphone (EP) that was attached to the insufflation port of the otoscope. Widefield imaging of the sample was provided by the otoscope integral digital imaging system that includes a visible light source, a fiber bundle (FB) and a small camera. All imaging experiments were conducted through the 4-mm-diameter exit aperture of the otoscope removable specula (ES).

A photograph of the imaging optics (Fig. 2) shows the various optical and mechanical components illustrated in Fig. 1 in the context of the otoscope handle (O). The tympanic membrane was modeled using a rubber membrane (M) stretched over one of the openings of a 11-mm-diameter, 26-mm-long aluminum cylinder. The membrane model was placed at the distal end of the ear canal of a silicon outer ear model (Nasco, Pneumatic ears, E), with the membrane surface perpendicular to the optical axis. Top inset in Fig. 2 provides an additional view of the earphone, ear model and the circular membrane when not in contact. Additional insets show the view of the otoscope camera (CM) with a 1-mm-square grid pattern replacing the rubber membrane, and a typical single-frame capture of the membrane axial position (discussed below).

### 3. Results

A crop from a typical two-dimensional raw data (Fig. 3), captured during 3 ms from a membrane excited by a harmonic 2.1 kHz acoustic wave, comprised of a time-series of individual spectral interferograms between reflections from the vibrating membrane and the (static) reference mirror. For system calibration, no scanning was performed by the mirror M1, allowing capturing acoustic vibrations from a single spectrally encoded line. The data was oversampled in both the horizontal spectral axis (by a factor of 3, see experimental setup) and in the time axis, where spectral acquisition rate (20 kHz) was approximately 9.5-times higher than the acoustic oscillation period (2.1 kHz). The reference arm delay was adjusted to produce moderate spectral modulation of approximately 0.71 modulation periods per sample location with spectral sampling of approximately 4 pixels per modulation period. A magnified view of a small region of interest (Fig. 3, white rectangle) of the raw data reveals the individual pixels that sample the periodic back-and-forth motion of the membrane. Using this data, the instantaneous axial displacement of each location on the sample was calculated by multiplying the phase shift  $\Delta\varphi$  between subsequent spectral interferograms (blue and green curves) by  $\lambda/4\pi$ , where  $\lambda$  denotes the central wavelength of the spectral band encoding the sample location.

For acquiring a two-dimensional vibration image, the scanning speed in the  $y$ -axis was 1.3 mm/s, adjusted for scanning the entire field of view ( $4.5 \times 4.5 \text{ mm}^2$ ) during 3.5 s with a total of 70,000 lines (20 kHz spectral acquisition rate) per single scan. This scan rate resulted in a single line capture every  $0.064 \mu\text{m}$  on the sample, equivalent to 110 spectral interferograms oversampling each single resolvable line ( $7 \mu\text{m}$  spatial resolution). The temporal oversampling of the acoustic oscillations depended on their frequency: 800 Hz waves were sampled by 25 spectra per vibration cycle with 4.4 vibration cycles captured for each sample line, while 6000 Hz acoustic waves were sampled by only 3.3 spectra per cycle with 33 vibration cycles per sample resolvable line. Data acquisition code (LabVIEW 2013) was upgraded from our previous system [12], now allowing continuous data streaming into a memory buffer without loss of data, and integrated control over the sound waveform. The acquired 4096-pixel spectra were low-pass filtered and divided into small spectral windows with 50% overlap for reducing artifacts caused by the window edges. The average phase of each window was calculated using Hilbert transform and the phase

difference  $\Delta\varphi_i$  between corresponding windows of subsequent spectra was used to calculate the axial displacement for each sample location using  $\Delta z_i = \Delta\varphi_i \lambda_i / 4\pi$ , where  $\lambda_i$  denotes the central wavelength for each window  $i$ . The processed data was stored as a series of discrete two-dimensional matrices that represent instantaneous axial displacements  $\Delta z$  for each sample location.

Snapshots representing the extremum positions of the circular membrane excited by a harmonic 1.4 kHz sound wave, computed using data processing with five different spectral window sizes (Fig. 4), demonstrate the trade-off between signal-to-noise ratio (SNR) and resolution. Because of the limited resolution of the spectrometer (four pixels per spectral modulation period), the minimal window size for sufficient phase measurement was 8-pixels, resulting in lateral resolution ( $19.7 \mu\text{m}$ ) in the horizontal axis lower by a factor of 2.8 compared to the optical lateral resolution ( $7 \mu\text{m}$ ). SNR was also relatively low (2.3), resulting in 11.7 nm axial resolution. Larger spectral windows improved the accuracy of the calculated phase differences and hence the axial resolution, up to 0.6 nm resolution for 128-pixel windows; however, lateral resolution was compromised (down to  $316.1 \mu\text{m}$ ) as window size significantly exceeds the bandwidth encoding each membrane location. We note, however, that acoustic waves often do not excite high spatial frequencies within the membrane, which allows averaging over neighboring pixels without sacrificing our ability to resolve different vibrational modes. We have found that using 32-pixel windows provided the best balance between lateral ( $79 \mu\text{m}$ ) and axial (2.8 nm) resolutions. Selected frames from a 13-snapshot movie (Visualization 1) of a membrane excited by a 1.5 kHz acoustic wave, which was processed using 32-pixel spectral windows, show (Fig. 5) the membrane oscillating at its fundamental circularly symmetric mode with uniform phases and an amplitude of approximately 50 nm.

The membrane exhibited more complex vibration patterns for higher excitation frequencies (Fig. 6); At harmonic excitations above 3000 Hz the relative phases became nonuniform across the membrane due to the superposition of several vibrational modes that produced traveling waves across the membrane (Visualization 2).

In order to test the sensitivity limits of the system for measuring small amplitude vibrations, we have imaged the membrane oscillations under 1400 Hz excitation with decreasing amplitudes controlled by the 0%–100% digital levels in the volume settings of the computer sound card. The vibration amplitudes were estimated from the vibration movies (20 kHz acquisition rate, 32-pixel spectral windows) as half the distance between the spatially averaged minimum-to-maximum displacements (Fig. 7). Error bars represent the averaged standard deviations of the noise across the images at the two extremum displacement frames. At volume setting level below 10% no periodic membrane displacements were observed and phase noise dominated the amplitude measurement. The linear dashed trendline demonstrates the nearly linear decrease in the measured oscillation amplitudes.

### 4. Discussion

Imaging the axial vibrational motion of a two-dimensional membrane requires the measurement of both amplitude and phase across its entire surface. The line-scanning approach presented in this work involves relatively simple optical setup with no need for rapid mechanical scanning. This approach is potentially advantageous over OCT by allowing shorter scanning times that would be critical for overcoming phase errors due to motion artifacts in *in vivo* application. Compared with full-field stroboscopic imaging, line imaging is advantageous by employing fiber-optic interferometry that is more robust and permits lower phase noise.

To be useful for most *in vivo* applications, the optical apparatus must be compact and easy to operate by clinicians. Modern state-of-the-art digital otoscopes are equipped with efficient white light source, light delivery by a compact fiber bundle, high-quality imaging optics and a digital camera, providing a direct, noninvasive visual access

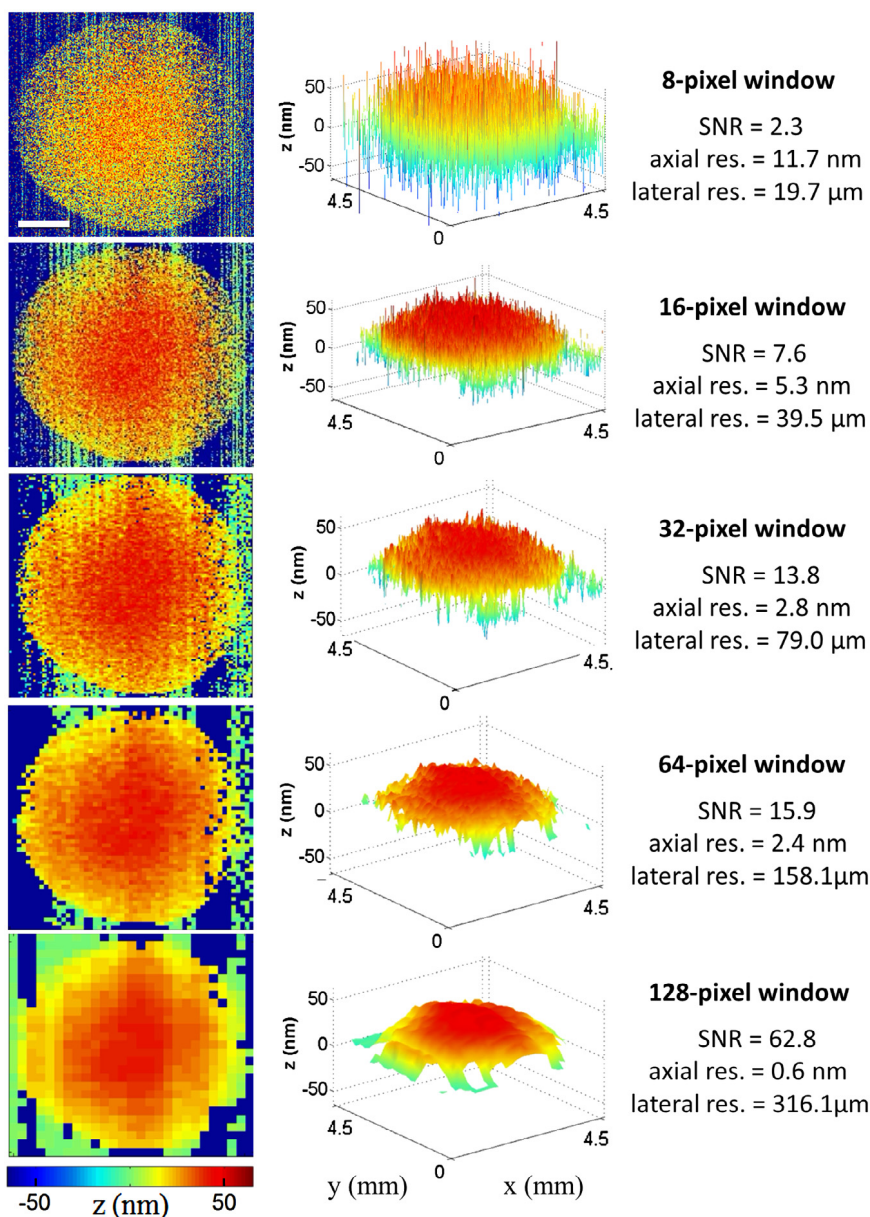


Fig. 4. Snapshots of the peak position of a membrane excited by 1.4 kHz harmonic wave, computed using different spectral window sizes. Scale bar represents 1 mm.

to the tympanic membrane. The system designed and characterized in this work presents a first step toward implementing functional vibration imaging into conventional otoscopes; our proof-of-concept apparatus allows excitation and imaging of membrane vibrations and was demonstrated effective on an ear model with nanometer-scale axial resolutions for a wide range of excitation frequencies (800–6000 Hz). The optical components in the imaging arm of the otoscope include a dichroic mirror, small lenses, a slow linear scanner, and a diffraction grating—all could be assembled into a compact add-on apparatus that could be attached to most commercially available otoscopes.

Some challenges remain before the device could be effectively used *in vivo*. First, a single scan required 3.5 s to complete, during which the otoscope must be kept motionless with respect to the tympanic membrane. Some methods could be employed to reduce motion artifacts, including scanning smaller regions of interest and by adjusting the reference mirror delay in real time to compensate for axial instabilities. We note that scan duration could be significantly shorter when optimizing temporal sampling: for example, the entire field of view of a membrane excited by a 2.5 kHz acoustic wave could be captured with

two vibration cycles per resolvable point in only 0.5 s total scan duration. In general, however, scanning and acquisition rates would depend on various parameters for achieving optimal SNR, including sample and spectrometer resolution, spectral modulation frequency, oscillation amplitude and window size. Second, the optical and optomechanical components may add substantial weight to the otoscope, which would reduce the usability of the device. Potential solutions to this problem may include the use of lightweight polymer optics and a more compact design with smaller diameter optics. Third, the tympanic membrane in patients has a typical angle of approximately  $45^\circ$  relative to the ear canal main axis [14] and can have more than  $10^\circ$  variation from person to person [15], resulting in non-uniform modulation frequencies across the spectral interferograms. We have previously proposed a technique [16] for overcoming an axial tilt in the spectrally encoded axis by using dispersion management at one of the arms of the Michelson interferometer, without modifying the imaging optics. Dispersion management, combined with otoscope rotation around its optical axis for aligning the membrane tilt gradient with the spectrally encoded line, will be incorporated into the system for future *in vivo* experiments. Finally, it is

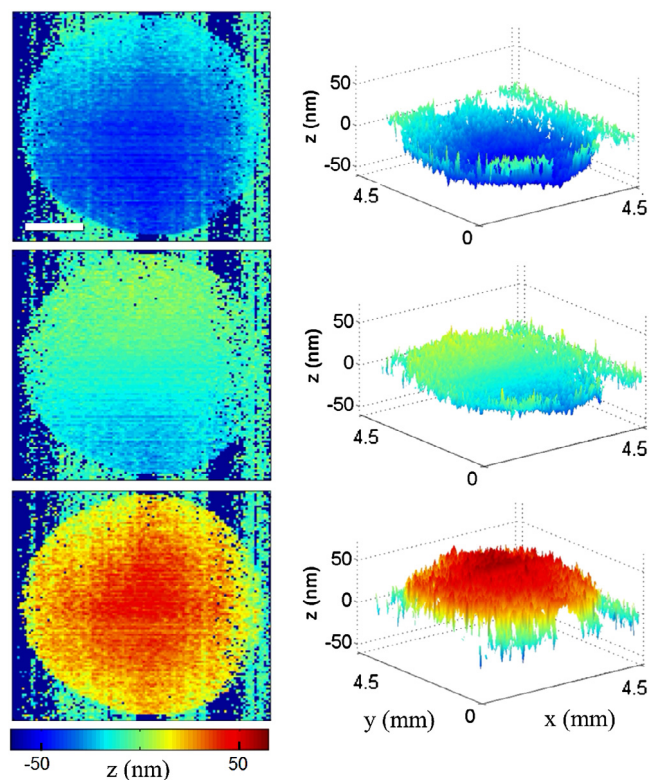


Fig. 5. Three frames from Visualization 1 showing the circular membrane oscillated at 1.5 kHz. Scale bar represents 1 mm.

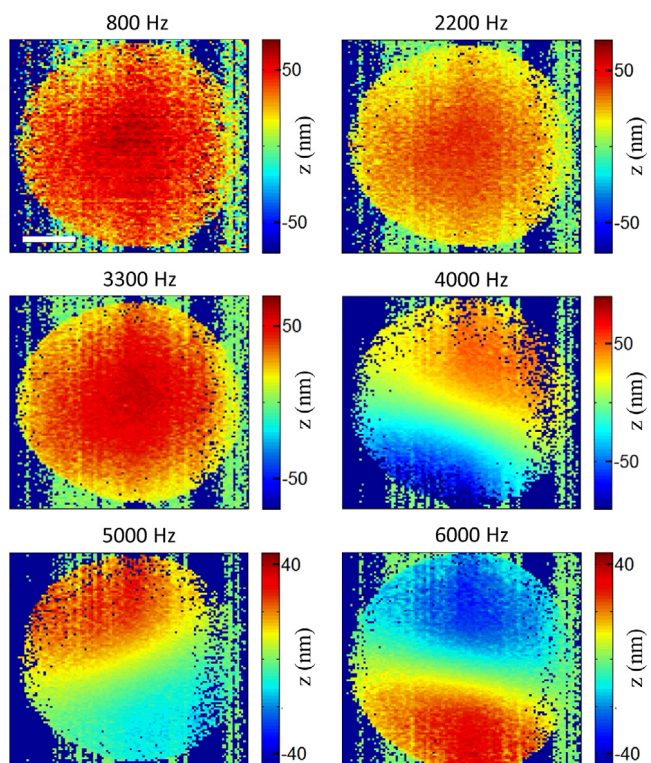


Fig. 6. Selected snapshots of a membrane excited by different acoustic frequencies. Scale bar represents 1 mm.

yet unclear how the tympanic membrane vibration modes are affected by the wide variety of physiological parameters and environmental factors. Once the system for *in vivo* imaging will be functional, various

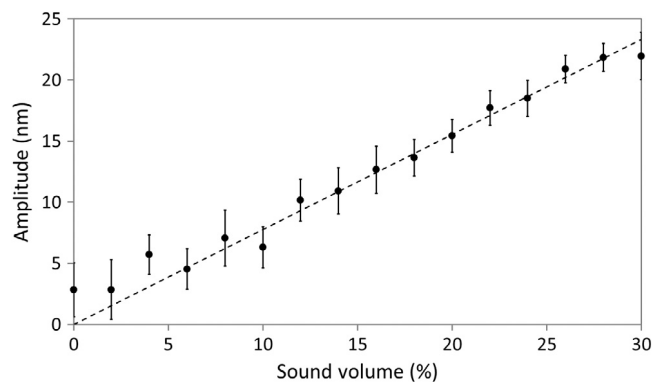


Fig. 7. Membrane oscillation amplitudes for different excitation sound intensities at 1.4 kHz.

fundamental studies could be conducted for determining the optimal scanning parameters, including sound wave frequency and amplitude, imaging rate, scanning speed, and relevant regions of interest within the field of view.

In summary, we designed and assembled a compact spectrally encoded interferometric system for imaging surface vibrations, and demonstrated the system by imaging a circular membrane within an ear model. Vibration amplitudes and phases with nanometer-scale axial resolutions were measured across a large  $4.5 \text{ mm} \times 4.5 \text{ mm}$  field of view. Future *in vivo* experiments will allow the study and development of the system for clinical diagnostics applications.

#### Funding Information

The study was supported in part by the Lorry Lokey Interdisciplinary Center for Life Sciences and Engineering.

#### Appendix A. Supplementary data

Supplementary material related to this article can be found online at <http://dx.doi.org/10.1016/j.optcom.2017.09.041>.

#### References

- [1] R.J. Roeser, M. Valente, H. Hosford-Dunn, *Audiology. Diagnosis*, Thieme, 2007.
- [2] S.T. Sinkkonen, J. Jero, A.A. Aarnisalo, Tympanic membrane perforation, *Duodecim* 130 (2014) 810–818.
- [3] R.P. Venekamp, M.J. Burton, T.M. van Dongen, G.J. van der Heijden, A. van Zon, A.G. Schilder, Antibiotics for otitis media with effusion in children, *Cochrane Database Syst. Rev. C* (2016) d009163.
- [4] G. Magliulo, D. Parrotto, B. Sardella, C. della Rocca, M. Re, Cavernous hemangioma of the tympanic membrane and external ear canal, *Am. J. Otolaryngol.* 28 (2007) 180–183.
- [5] L. Michaels, Origin of congenital cholesteatoma from a normally occurring epidermoid rest in the developing middle ear, *Int. J. Pediatr. Otorhinolaryngol.* 15 (1988) 51–65.
- [6] J.A. Beyea, S.A. Rohani, H.M. Ladak, S.K. Agrawal, Laser doppler vibrometry measurements of human cadaveric tympanic membrane vibration, *J. Otolaryngol. Head Neck Surg.* 42 (2013) 17.
- [7] J.J. Rosowski, H.H. Nakajima, S.N. Merchant, Clinical utility of laser-doppler vibrometer measurements in live normal and pathologic human ears, *Ear Hear* 29 (2008) 3–19.
- [8] A. Burkhardt, L. Kirsten, M. Bornitz, T. Zahnert, E. Koch, Investigation of the human tympanic membrane oscillation *ex vivo* by doppler optical coherence tomography, *J. Biophotonics* 7 (2014) 434–441.
- [9] J.T. Cheng, A.A. Aarnisalo, E. Harrington, M. del S. Hernandez-Montes, C. Furlong, S.N. Merchant, J.J. Rosowski, Motion of the surface of the human tympanic membrane measured with stroboscopic holography, *Hear. Res.* 263 (2010) 66–77.
- [10] D. Yelin, B.E. Bouma, J.J. Rosowski, M.E. Ravicz, G.J. Tearney, Interferometric spectrally encoded endoscopy, in: *Biomedical Optics*, Optical Society of America, 2008, p. BTuB2.

- [11] D. Yelin, B.E. Bouma, J.J. Rosowsky, G.J. Tearney, Doppler imaging using spectrally-encoded endoscopy., *Opt. Express* 16 (2008) 14836–14844.
- [12] O. Ilgayev, D. Yelin, Phase-sensitive imaging of tissue acoustic vibrations using spectrally encoded interferometry, *Opt. Express* 21 (2013) 19681–19689.
- [13] M. Merman, A. Abramov, D. Yelin, Theoretical analysis of spectrally encoded endoscopy, *Opt. Express* 17 (2009) 24045–24059.
- [14] S.A. Gelfand, *Hearing: An Introduction to Psychological and Physiological Acoustics*, fifth ed., 2010.
- [15] J.P. Fay, S. Puria, C.R. Steele, The discordant eardrum, *Proc. Natl. Acad. Sci.* 103 (2006) 19743–19748.
- [16] M. Merman, D. Yelin, Dispersion management for controlling image plane in fourier-domain spectrally encoded endoscopy, *Opt. Express* 19 (2011) 4777.